



Synthesis and characterization of guanine-functionalized mesoporous silica [SBA-16-G]: a metal-free and recyclable heterogeneous solid base catalyst for synthesis of pyran-annulated heterocyclic compounds

Radha Gupta¹ · Samaresh Layek¹ · Devendra Deo Pathak¹ 

Received: 1 October 2018 / Accepted: 28 November 2018
© Springer Nature B.V. 2018

Abstract

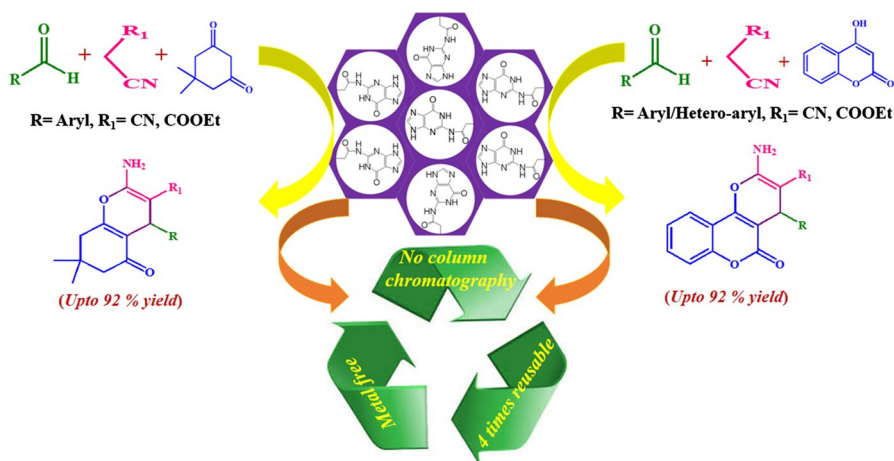
The synthesis of a new solid base catalyst, i.e., guanine-functionalized mesoporous silica [SBA-16-G], is described. The synthesized catalyst has been fully characterized by FTIR, solid state ¹³C NMR, TGA, XRD, BET, FESEM, EDAX, CHNS elemental analysis, CO₂-TPD, and TEM techniques. The surface area and the basicity of the synthesised [SBA-16-G] were found to be 524 m²/g and 3.230 mmol/g, respectively, based on BET and CO₂-TPD analysis. The catalytic activity of the synthesized catalyst has been explored in the synthesis of a series of biologically and pharmaceutically active pyran-annulated heterocyclic compounds from a one-pot three-component reaction of an aromatic aldehyde, malononitrile/ethyl cyanoacetate, and a C–H activated acidic compound, in the presence of a catalytic amount (10 wt%) of [SBA-16-G]. The catalyst is metal-free, easy to synthesize and to isolate from the reaction mixture, and recycled up to four times without significant loss of catalytic activity.

Electronic supplementary material The online version of this article (<https://doi.org/10.1007/s11164-018-3693-5>) contains supplementary material, which is available to authorized users.

✉ Devendra Deo Pathak
ddpathak@iitism.ac.in

¹ Department of Applied Chemistry, Indian Institute of Technology (Indian School of Mines), Dhanbad, Jharkhand 826004, India

Graphical abstract



Keywords Guanine-functionalized SBA-16 · Pyran · Metal-free · Heterogeneous catalysis · Solid base

Introduction

A chemical reaction can be triggered by an acidic or a basic catalyst in a catalytic cycle [1]. Over the last few decades, solid bases have been the subject of intense investigation in the field of catalysis [2–5]. Pines and Haag [6] reported the use of sodium alumina as a solid base catalyst for the first time in 1958, for the isomerisation of alkenes. Since then, the scope of solid-base catalysts has been extended to a variety of chemical reactions, such as the oxidation of thiol [7], the synthesis of fine chemicals [8], degradation reactions [9], biomass conversion [10], multi-component synthesis [11], and the transesterification of trioleins and the production of biofuels [12, 13]. Many solid-base catalysts, such as DABCO [11], K_2CO_3 -loaded alumina [12], metal oxides (MgO , CaO , SrO , BaO , LaO_2 , ThO_2 , ZrO_2 , ZnO , TiO_2), zeolites, supported alkali metal ions, clay minerals, non-oxides [14], CaO/MgO [15], $K/BC-Fe_2O_3$ [16], etc., have been used as heterogeneous catalysts for the synthesis of a diverse range of value-added chemicals.

Mesoporous silicas (MSs) were discovered in 1969 [17, 18]. MSs have a large surface area, high pore volume, and uniform pore radius. As a consequence, these materials have been used in drug delivery [19], sorption [20], energy storage [21], catalysis [22], etc. MSs are thermally robust and ideally suitable for functionalization with suitable organic scaffolds to yield functionalized MSs. The functionalized MSs have opened up new vistas of research in catalysis, sensors, energy, and biomedical fields [23–31]. Presently, there is a renaissance of interest in the synthesis

and applications of functionalized or grafted MSs [32–36]. Aspartic acid, polyethyl-*enimine*, and β -cyclodextrin-functionalized MSs have recently been reported [37].

Pyran-annulated coumarins are an integral part of several pharmaceuticals and are abundant in nature [38]. These coumarin scaffolds display a variety of biological activities [39]. Furthermore, these compounds exhibit a wide spectrum of properties, such as diuretic, analgesic, myorelaxant [40], anticoagulant [41], anticancer [42], antifungal [43], antibacterial [44], antirheumatic [44], antiHIV [45] and antitumor [46]. A few biologically active pyran-annulated heterocycles and their properties are shown in Fig. 1. Apart from these applications, these compounds are also useful in the treatment of neurodegenerative ailments, i.e., Alzheimer's disease, amyotrophic parallel sclerosis, and Huntington's and Parkinson's diseases [46–50]. Other miscellaneous applications of these compounds include beauty care products and pigments [51], photoactive materials, etc [52].

A literature survey reveals that several acid/base catalysts, such as DMAP [53], urea [54], DBU [55], TBBDA and PBBS [56], $(\text{NH}_4)_2\text{HPO}_4$ [57], heteropoly acids [58], basic ionic liquid [59], nano-ZnO [60], $\text{C}_{19}\text{H}_{42}\text{BrN}$ [61], magnetic nanocatalyst [62], hydroxyapatite [63], per-6-amino- β -cyclodextrin [64], nano- Al_2O_3 [65], $\gamma\text{-Fe}_2\text{O}_3 @ \text{Cu}_3\text{Al-LDH-TUD}$ [66]. etc., have been used for the synthesis of pyran-annulated coumarin derivatives. All these methods suffer from one of a number of drawbacks, such as high temperature, use of hazardous solvents and metals, tedious work-up, recyclability of catalysts and low yield of products. In order to circumvent these inherent problems, currently there is much emphasis on the design and development of green, sustainable, and metal-free catalysts for organic synthesis [67–70]. In continuation of the earlier work [37, 71] and our

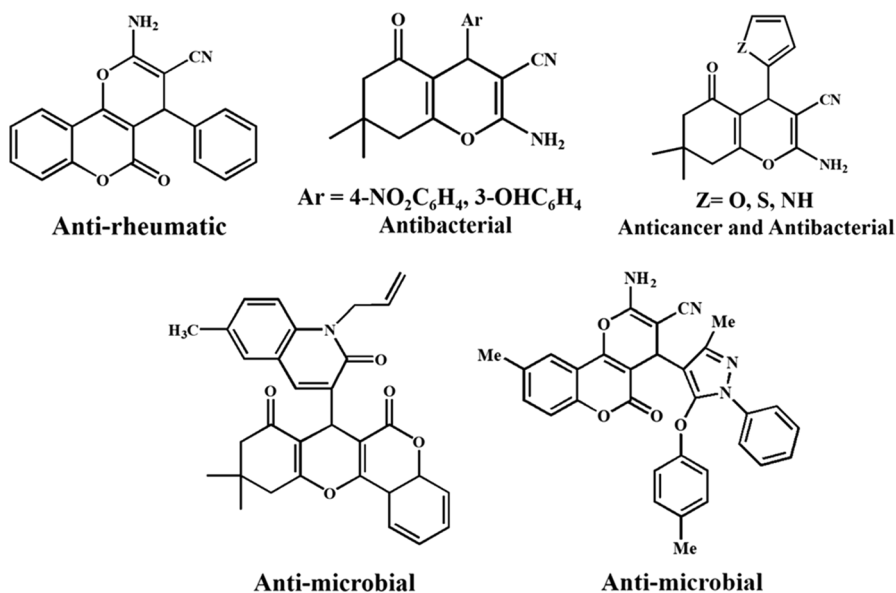


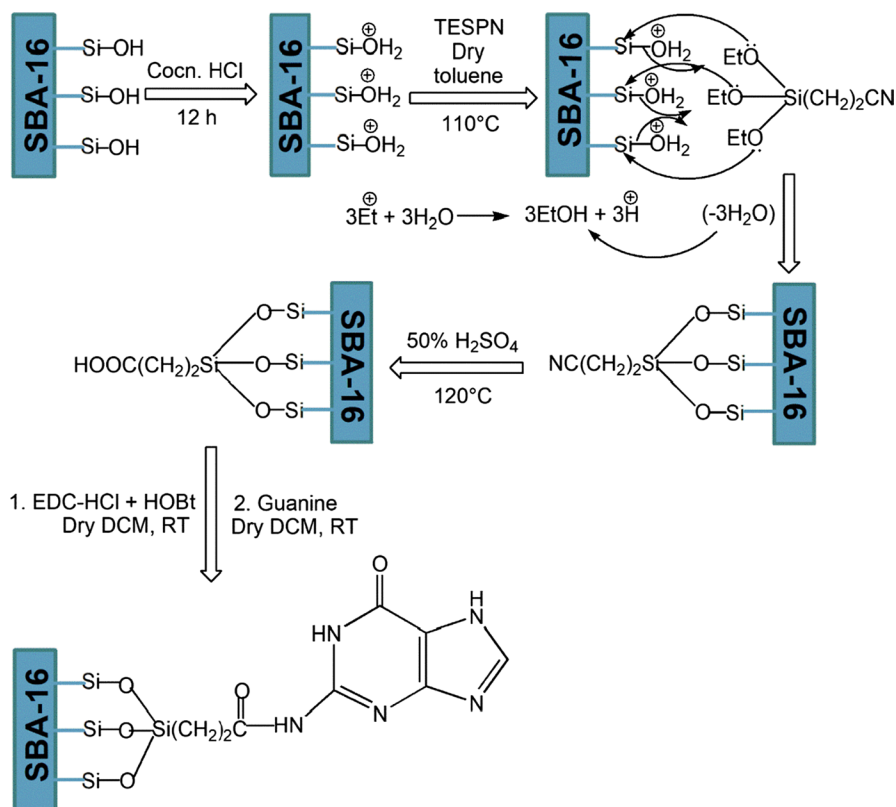
Fig. 1 Some representative examples of active pharmacology synthetic pyran-annulated heterocyclic compounds

current interest on metal-free catalysis, we report the synthesis of a new solid base, i.e. guanine-functionalized SBA-16 (Scheme 1) and its application as a heterogeneous catalyst for the synthesis of pyran-annulated heterocyclic compounds (Scheme 2).

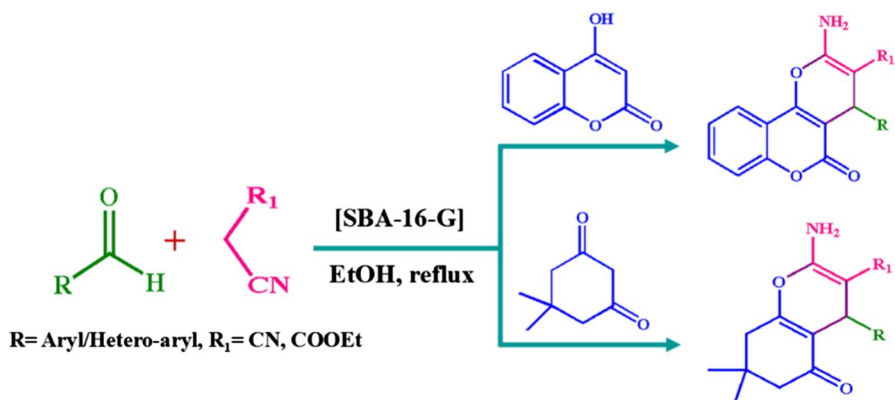
Experimental

Materials and reagents

Tetraethoxysilane (TEOS, $\geq 99\%$), 3-(triethoxysilyl)-propionitrile ($\geq 98\%$), and pluronic F127 ($\text{EO}_{106}\text{PO}_{70}\text{EO}_{106}$) were purchased from Sigma Aldrich. 1-hydroxy-benzotriazole hydrate (HOBt, $\geq 98\%$), 4-hydroxycoumarin, and 1-(3-dimethyl amino propyl)-3-ethyl carbodiimide hydrochloride (EDC-HCl, $\geq 98\%$), were procured from Avra Chemicals. Guanine ($\geq 98\%$) was purchased from Alfa Aesar. Toluene ($\sim 98\%$), hydrochloric acid ($\text{HCl} \sim 37\%$), petroleum



Scheme 1 Proposed scheme for the synthesis of [SBA-16-G]



Scheme 2 Proposed reaction scheme for the synthesis of pyran-annulated heterocyclic compounds

ether ($\geq 98\%$), ethylacetate ($\geq 98\%$), thin-layer chromatographic (TLC) plates, dichloromethane (DCM), and sulfuric acid ($\sim 98\%$) were procured from Merck India. All those chemicals were used without further purification.

Synthesis of [SBA-16-G]

SBA-16 was synthesized using the well-known reported procedure [72]. An amount of 0.0248 mol (4.0 g) of pluronic F127 was dissolved in 30.0 mL of water and 120.0 mL of 2 M HCl solution and stirred at 35 °C. Then, 10.6 mL of TEOS was added into that solution and stirred at the same temperature for 20 h. The mixture was aged at 80 °C for 2 days without stirring. The solid product was recovered, washed, and air-dried at 130 °C for 6 h. Calcination was carried out at 500 °C for 8 h to remove the surfactant at a heating rate of 5 °C/min for 3 h. Before functionalization, the formed material was refluxed in concentrated HCl for 12 h to activate the surface silanol (Si-OH) groups [37, 71]. Thereafter, the material was made acid-free by washing with distilled water three times and dried under vacuum at 100 °C for 24 h.

The SBA-16-CN was prepared following the reported procedure [37, 71]. Initially, 3-(triethoxysilyl)-propionitrile (0.1 mol) and 3 g of activated SBA-16 in dry toluene (50 mL) were mixed and stirred in a round-bottom flask at 110 °C for 18 h, resulting in cyano-functionalized SBA-16. It was repeatedly treated with dry toluene and dried at 125 °C under reduced pressure. Then, SBA-16-CN was refluxed with 50 mL of $\sim 50\%$ H_2SO_4 at 120 °C for 18 h and afforded SBA-16-COOH [37, 71]. Then, the as-synthesized SBA-16-COOH was washed extensively with distilled water to make it free from acid and dried at 110 °C under reduced pressure. Finally, [SBA-16-G] was synthesized when 0.3 mol of EDC-HCl and 0.3 mol HOBt were mixed in 3.0 g of SBA-16-COOH in 25 mL of dry DCM at room temperature (RT) followed by the treatment with 0.3 mol of guanine in 25 mL of dry DCM at RT.

General procedure for catalytic experiment

Well-dispersed 10 wt% [SBA-16-G] in 4 mL ethanol, prepared by sonication for 10 min, was added to the combined mixture of 4-chlorobenzaldehyde (1 mmol) and malononitrile (1 mmol). The resultant reaction mixture was stirred at RT for 20 min and the reaction was monitored using TLC. Thereafter, 4-hydroxycoumarin (1 mmol) was added to the reaction mixture and heated at reflux for 4.5 h. After completion of the reaction, the reaction mixture was cooled to room temperature. After this, the reaction mixture was filtered. The residue was washed with hot ethanol and the catalyst was separated and the pure product was found by the evaporation of the ethanol. The as-synthesized product was analyzed by FTIR, ^1H NMR, and ^{13}C NMR and the data are given in the supplementary information (SI).

Characterizations

Fourier-transform infrared (FTIR) spectroscopic analyses were carried out on a FTIR spectrometer (Perkin Elmer, Spectrum 2000) using KBr pellet method. Thermogravimetric analysis (TGA; NETZSCH STA-449f3, Jupiter) was executed on a thermal analyser in the temperature range 25–900 °C at a heating rate of 5 °C/min in N_2 flow. X-ray diffraction (XRD) patterns were determined using a Thermal ARL X-ray diffractometer (CuK_α radiation). The BET surface area measurements were carried out at 77 K with a Nova 3200e (Quantachrome, USA). Field emission scanning electron microscopic (FESEM) analyses with energy-dispersive X-ray analysis (EDAX; Supra 55, Zeiss, Germany), CHNS elemental analysis, CO_2 -temperature programmed desorption (CO_2 -TPD) were analyzed by BEL's new fully-automated catalyst analyzer and transmission electron microscopic (TEM) analyses (JEM-2100; JEOL, Japan) were performed to obtain clear evidence about the pre- and post-material surface properties of SBA-16 and [SBA-16-G]. The solid-state ^{13}C spectra were analyzed using a JEOL ECA400 MHz instrument operated with 4 mm CD/MAS at RT. For catalytic reactions, the reaction product was collected and analyzed using FTIR, ^1H NMR and a ^{13}C NMR spectrometer operating at 400 MHz and 500 MHz, using $\text{DMSO-}d_6$, CDCl_3 as the solvent and tetramethylsilane as an internal standard. δ values are reported in parts per million (ppm) and coupling constants (J) in Hertz (Hz). The melting point was recorded on a Buchi melting point apparatus.

Results and discussion

Synthesis and characterizations of pre- and post-functionalized materials

The starting material, SBA-16, was synthesized by the reported method [73]. The synthesis of guanine-functionalized [SBA-16-G] is outlined in Scheme 1. The synthesized material was used in the heterogeneous catalytic reaction.

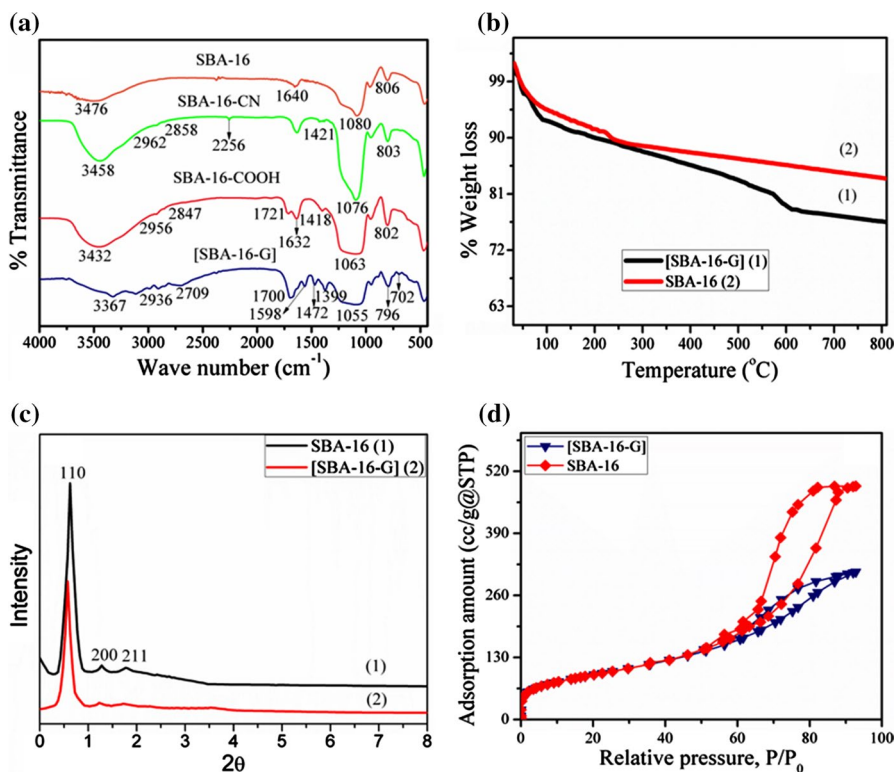


Fig. 2 a FTIR spectra of SBA-16, SBA-16-CN, SBA-16-COOH, and [SBA-16-G]; b TGA plots of SBA-16 and [SBA-16-G]; c XRD spectra; and d surface area measurements of SBA-16 and [SBA-16-G]

The FTIR spectrum of SBA-16 (Fig. 2a) shows a broad -OH stretching band at 3476 cm^{-1} . The symmetric and asymmetric Si-O-Si stretching vibrational modes were observed at 806 cm^{-1} and 1080 cm^{-1} , respectively [37]. A band at 1640 cm^{-1} was assigned to the bending mode of Si-OH [37]. SBA-16-CN showed a new peak at 2256 cm^{-1} which is due to the attachment of the -CN group in the product. The product SBA-16-COOH showed a broad band of $\nu\text{-OH}$ at 3432 cm^{-1} , -CH_2 symmetric and asymmetric stretching bands near 2847 cm^{-1} and 2956 cm^{-1} , and a band at 1063 cm^{-1} due to the asymmetric Si-O-Si stretching mode. The -OH bending of the Si-OH group is shifted from 1640 to 1632 cm^{-1} , a scissoring vibrational mode of the -CH_2 group appeared at 1418 cm^{-1} and a symmetric Si-O-Si stretching band at 802 cm^{-1} . A typical band of the -C=O stretching vibration of the carboxylic acid group appears at 1721 cm^{-1} . This suggests the successful formation of carboxylic acid moieties on the material. On the other hand, for [SBA-16-G], the Si-OH band was shifted from 3432 to 3367 cm^{-1} , -CH_2 symmetric and asymmetric stretching bands shifted to 2709 cm^{-1} and 2936 cm^{-1} respectively, asymmetric Si-O-Si stretching band shifted to 1055 cm^{-1} , scissoring vibrational mode of the -CH_2 group

shifted to 1399 cm^{-1} , symmetric Si–O–Si stretching band shifted to 796 cm^{-1} , and $\text{C}=\text{O}$ stretching vibration of the carboxylic acid group shifted to 1700 cm^{-1} . Moreover, a N–H bending vibration appears at 702 cm^{-1} and the bands appearing at 1598 cm^{-1} and 1472 cm^{-1} confirm the presence of C=N and C–N stretching bands in [SBA-16-G] [74].

The TGA of both SBA-16 and [SBA-16-G] are shown in Fig. 2b. Initially, the weight loss ($\sim 5\%$) up to $150\text{ }^\circ\text{C}$ is ascribed to the removal of surface-adsorbed water molecules from both materials [74]. A significant weight loss ($\sim 25\%$) was observed in the temperature range between 275 and $575\text{ }^\circ\text{C}$ for [SBA-16-G], owing to the decomposition of the guanine moiety present in the material.

Figure 2c shows XRD spectra of both the pre- and post-functionalized materials. The SBA-16 shows the characteristic peaks at 2θ values 0.618° , 1.289° , and 1.778° corresponding to the 110, 200, and 211 planes, respectively, consistent with the reported data [73]. In the guanine-functionalized SBA-16, the intensities of all three peaks were slightly diminished and shifted towards lower 2θ values, presumably due to functionalization with the guanine.

The BET surface area measurements data for SBA-16 and [SBA-16-G] are summarized in Table 1 and the hysteresis loops shown in Fig. 2d. Table 1 indicates that SBA-16 has a large surface area ($781\text{ m}^2/\text{g}$), pore diameter ($11.9\text{ nm cm}^3/\text{g}$) and pore volume ($0.86\text{ cm}^3/\text{g}$) [75]. However, after guanine-functionalization, the surface area, pore diameter and pore volume ($524\text{ m}^2/\text{g}$, 9.2 nm , and $0.77\text{ cm}^3/\text{g}$, respectively) were decreased. This occurs because the guanine moieties occupy space in the pores of SBA-16.

Both the FESEM and TEM images for SBA-16 and [SBA-16-G] are depicted in Fig. 3. Figure 3a reveals that SBA-16 is a well-developed, spherical, and crystalline material. The FESEM image of [SBA-16-G] shows an agglomerated morphology (Fig. 3b). The TEM image of SBA-16 indicates a sheet-like surface morphology and ordered lattice arrays of the virgin material (Fig. 3c) [75]. However, after guanine functionalization, no significant changes were observed in the ordered lattice arrays (Fig. 3d). Therefore, it is inferred from the TEM image that the ordered structure was retained and the guanine functionalities were deposited in the pores of SBA-16.

The guanine-functionalization onto SBA-16 was confirmed by the solid-state ^{13}C NMR (Fig. 4). This shows strong peaks at δ 8.1, 14.6, 28.3, and 43.9 corresponding to the presence of aliphatic carbons of the chain attached to the silica in [SBA-16-G] [37]. The peaks at δ 178.2, and δ 108.8 are assigned to the $\text{C}=\text{O}$ of the amide linkage and the C–N bond, respectively. Moreover, strong signals at around δ 158.6 and δ 160.5 may be attributed to different carbons of the guanine

Table 1 BET surface area, average pore diameter, and total pore volume of SBA-16 and [SBA-16-G]

Entry	Materials	BET surface area (m^2/g)	Average pore diameter (nm)	Total pore volume (cm^3/g)
1.	SBA-16	781	11.9	0.86
2.	[SBA-16-G]	524	9.2	0.77

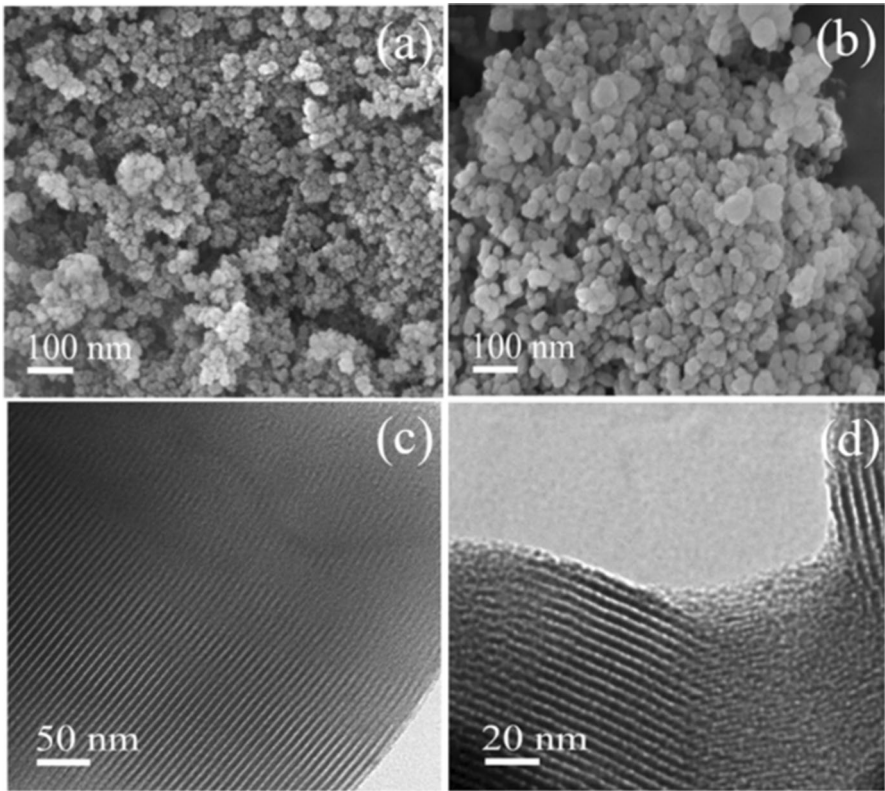


Fig. 3 FESEM of SBA-16 (a) and [SBA-16-G] (b); TEM of SBA-16 (c) and [SBA-16-G] (d)

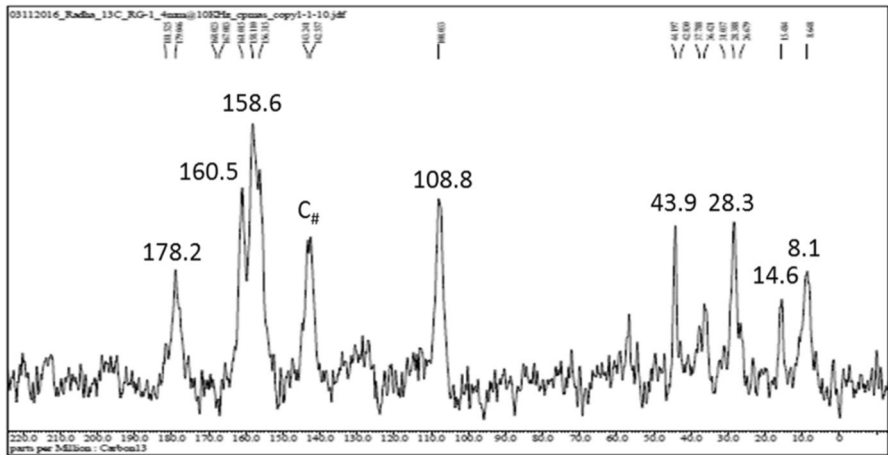


Fig. 4 Solid-state ^{13}C NMR spectrum of [SBA-16-G]

moiety. A signal at δ 144 is assigned to the residual benzene which was used as a solvent during the synthesis of [SBA-16-G].

The basicity of the SBA-16 and [SBA-16-G] were measured using the CO₂-TPD technique. The CO₂-TPD profile of SBA-16 showed three peaks, at 148 °C, 308 °C, and 695 °C, as denoted by α , β and γ , respectively (Fig. 5) [76]. The temperature and area of the CO₂ desorption peaks can be used to access the apparent strength and quantity of the basic property of the materials. Therefore, three peaks in the CO₂-TPD of SBA-16 were attributed to weak, moderate and strong basic sites, respectively. However, CO₂-TPD of [SBA-16-G] showed four intense peaks, at 197 °C, 407 °C, 498 °C and 715 °C, as denoted by α' , β' , δ' and γ' , respectively. Moreover, a comparison of CO₂-TPD studies of SBA-16 and [SBA-16-G] showed that the [SBA-16-G] exhibited an additional strong and new peak δ' at 498 °C and the shifting of the remaining peaks at 197 °C (α'), 407 °C (β') and 715 °C (γ'), which indicated that, after guanine functionalization, the basicity has been substantially increased, from 0.458 to 3.230 mmol/g.

Catalytic studies

The catalytic activity of the synthesized [SBA-16-G] was investigated for the synthesis of the pyran-annulated heterocyclic compound, as shown in Scheme 2.

In order to optimize the reaction conditions, different screening parameters, such as catalyst loading, solvent and time were carried out and their results are shown in Table 2. The reaction of 4-chlorobenzaldehyde (1 mmol), malononitrile (1 mmol) and 4-hydroxycoumarin (1 mmol) in ethanol (4 mL) was chosen as a model reaction. In the absence of the catalyst, at RT, no desired product was found after 18 h (Table 2, entry 1). Similarly, in the absence of the catalyst even at 80 °C, no product was formed (Table 2, entry 2). However, in the presence of 2 wt% of [SBA-16-G]

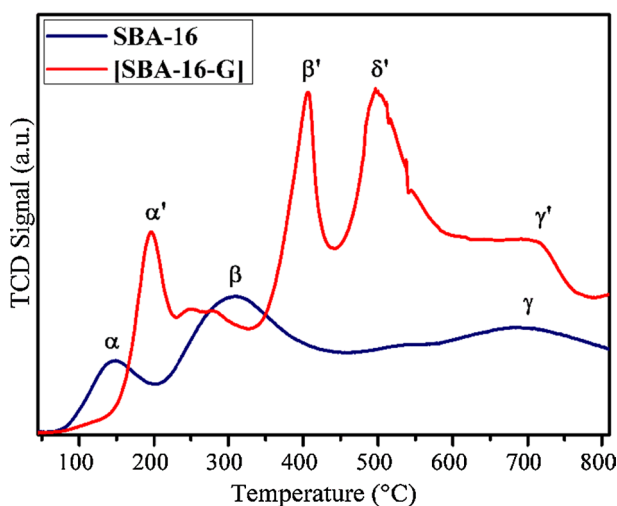
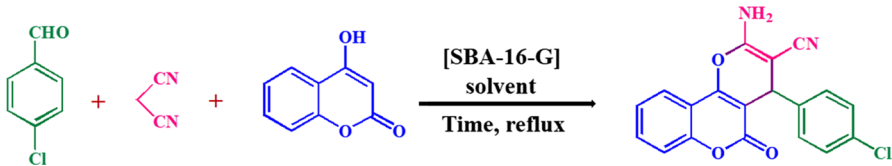


Fig. 5 CO₂-TPD profile for SBA-16 (a) and [SBA-16-G] (b)

Table 2 Optimization of reaction conditions for the synthesis of pyran-annulated heterocyclic compound from 4-chlorobenzaldehyde, malononitrile, and 4-hydroxycoumarin


Entry	Catalyst (wt%)	Solvent	Time (h)	Temp. (°C)	Yield (%) ^a
1	–	EtOH	18	RT	n.r.
2	–	EtOH	18	80	Trace
3	2	EtOH	10	80	65
4	5	EtOH	7	80	88
5	10	EtOH	5	80	92
6	10	CH ₃ CN	19	80	40
7	10	H ₂ O	15	100	35
8	10	Benzene	9.5	100	51
9	10	EtOH:H ₂ O (1:1)	10	80	72
10	10	Ethylacetate	16	80	n.r.
11	10	THF	18	80	27
12	10 (Guanine)	EtOH	5	80	75

Reaction conditions: aldehyde **1** (1 mmol), ethyl cyanoacetate/malononitrile **2** (1 mmol) and dimedone **3b** (1 mmol)

^aIsolated pure yield; *n.r.* no reaction

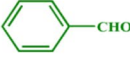
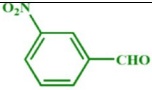
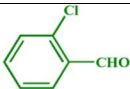
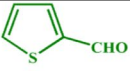
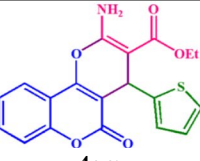
in ethanol (4 mL) at refluxing condition, the desired product was formed in 65% yield (Table 2, entry 3). In the presence of 5 wt% of [SBA-16-G] in ethanol (4 mL) at 80 °C, the product was formed at 88% in yield (Table 2, entry 4). In the presence of 10 wt% of [SBA-16-G] in ethanol (4 mL) at refluxing condition, 92% yield of product was obtained within 5 h (Table 2, entry 5). Thereafter, in order to optimize the effect of the solvent, the reaction was performed in various solvents, such as ethanol, CH₃CN, C₆H₆, H₂O, ethanol:H₂O, ethylacetate, THF, etc. (Table 2, entries 6–11). When the reaction was carried out in benzene or ethanol:H₂O, only 51% and 72%, respectively, of the desired product were formed (Table 2, entries 8, 9). However, in pure ethanol, the product yield increased to 46% and 25%, respectively (Table 2, entries 8, 9). In the presence of CH₃CN and H₂O, the desired products were obtained at only 40% and 35%, respectively (Table 2, entries 6, 7). In the presence of ethylacetate, no product was found after 16 h, while in THF, only 27% of the desired yield was formed after 18 h (Table 2, entries 10, 11). Finally, in the presence of just guanine as the catalyst, in ethanol (4 mL) at 80 °C, 75% of the desired yield was found (Table 2, entry 12).

After the optimization conditions, to check the scope and generality of the present catalyst, a series of reactions were carried out using different

Table 3 Aromatic aldehydes, malononitrile and 4-hydroxycoumarin used for the synthesis of dihydropyrano[3,2-c]chromene derivatives catalyzed by [SBA-16-G]

<p>R = Aryl/Hetero-aryl R₁ = CN, COOEt</p>					
Entry	Aromatic aldehydes	Product	Time (h)	Yield (%) ^a	Mp. °C
1		 4aa	5	92	267–269 [264–266] ⁵³
2		 4ab	3.5	91	253–255 [254–256] ⁵⁴
3		 4ac	9	92	257–259 [258–260] ⁵³
4		 4ad	1	92	230–232 [234] ⁵⁴
5		 4ae	6	91	259–261 [261–262] ⁵⁴
6		 4af	1.5	88	252–254 [254–256] ⁵⁴
7		 4ag	5	90	139–141 [142–144] ⁵³

Table 3 (continued)

8		 4ah	3	91	196–198 [194–195] ⁵³
9		 4ai	4	79	186–188 [187–189] ⁵³
10		 4aj	4.5	83	238–240 [242–245] ⁵³
11		 4ak	2	87	237–239 [241–244] ⁴⁸
12		 4al	4.5	70	214–216 [209–212] ⁵³
13		 4am	3	89	199–201 [205] ⁶⁰

Reaction conditions: aldehyde **1** (1 mmol), ethyl cyanoacetate/malononitrile **2** (1 mmol) and 4-hydroxycoumarin **3a** (1 mmol) and 10 wt% [SBA-16-G] used as catalyst in 4 mL ethanol at room temperature followed by refluxing condition

^aIsolated yield

substituted aldehydes, malononitrile/ethyl cyanoacetate, and 4-hydroxycoumarin/dimedone/4-hydroxyindole under optimizations condition,s and their results were summarized in Tables 3 and 4. The reactions of malononitrile with benzaldehyde and 4-hydroxycoumarin were executed under the same reaction conditions to get the desired product **4ab** in 90% yield. The reactions of the aldehydes with electron-donating groups such as, $-\text{CH}_3$, $-\text{OCH}_3$ etc. (Table 2, entries 4ac, 4ad) as well as electron-withdrawing groups, i.e. $-\text{Cl}$, $-\text{F}$, $-\text{NO}_2$ (Table 3, entries 4aa,

Table 4 Aromatic aldehydes, ethyl cyanoacetate, and diketones used for the synthesis of chromene derivatives catalyzed by [SBA-16-G]

Entry	Dimedone	Product	Time (h)	Yield (%) ^a	Mp. °C
1		 4ba	2.5	92	214–216 [212–214] ⁵⁴
2		 4bb	2.5	91	202–204 [205–206] ⁵⁴
3		 4bc	4	90	142–144 [139–142] ⁵³
4		 4bd	3	91	145–147 [144–146] ⁵³
5		 4be	1.5	86	159–161 [154–156] ⁵³
6		 4bf	1	90	169–171
7		 4bg	3.5	90	141–143

Reaction conditions: aldehyde **1** (1 mmol), ethyl cyanoacetate/malononitrile **2** (1 mmol) and dimedone **3b** (1 mmol) and 10 wt% [SBA-16-G] used as catalyst in 4 mL ethanol at room temperature followed by refluxing condition

^aIsolated yield

4ae, **4af**) also gave the desired products in very good yield under optimization conditions. Similarly, the reactions of ethyl cyanoacetate with aromatic aldehydes



Scheme 3 Three-component reaction of malononitrile, 4-chlorobenzaldehyde and 4-hydroxyindole

Table 5 A comparative study of catalysts for synthesis of pyran-annulated heterocycles from the reaction of 4-chlorobenzaldehyde, malononitrile, and 4-hydroxycoumarin

Entry	Catalyst	Solvent/conditions	Time	Yield (%)	References
1	Urea (10 mol %)	EtOH:H ₂ O	7 h	93	[54]
2	TBBDA and PBBS (18 mol% and 0.1 g)	EtOH:H ₂ O	3.25 h and 3 h	89 and 90	[56]
3	Nano Al ₂ O ₃	EtOH	5 h	80	[65]
4	γ -Fe ₂ O ₃ @Cu ₃ Al-LDH-TUD	Solvent-free	18 min	90	[66]
5	SBA-16	EtOH	24 h	08	This work
6	[SBA-16-G]	EtOH	5 h	92	This work

and 4-hydroxycoumarin were also carried out under the same reaction conditions and the products were obtained in high yield (Table 3, entries 4ag–4al). Under the optimized conditions, the reaction of ethyl cyanoacetate with heterocyclic aldehyde, i.e., thiophene-2-carbaldehyde and 4-hydroxycoumarin, was also carried out to give the product in 89% yield (Table 3, entry 4am). Isolated products were fully characterized by standard spectroscopic methods and their data and spectra are given in the SI (Figs. S2–S26).

The present study was also successful when the reactions of substituted aromatic aldehyde, malononitrile and dimedone were carried out under similar reaction conditions and afforded the corresponding three-component condensation products in very good yields (Table 4, entries 4ba, 4bb). The reactions of dimedone with substituted aromatic aldehydes and ethyl cyanoacetate were also analyzed and the desired product were found in good yield under optimized reaction conditions (Table 4, entries 4bc–4bg). It is important to describe that in all cases, aromatic aldehydes substituted with either electron-withdrawing groups or electron-donating groups underwent the reaction very smoothly and gave the desired products in good to excellent yields under the optimized conditions (Table 4). We have also carried out the reaction of malononitrile, 4-chlorobenzaldehyde and 4-hydroxyindole under optimized conditions and it afforded 76% in yield (Scheme 3). Isolated products were fully characterized by FTIR, ¹H NMR and ¹³C NMR spectroscopic methods and their data and spectra are given in SI (Fig. S27–S41). Furthermore, Table 5 also indicates the comparison of the activity of the different reported catalysts [54, 56, 65, 66], with that of the synthesized [SBA-16-G] catalyst. We observed that the current [SBA-16-G] catalyst gives the best

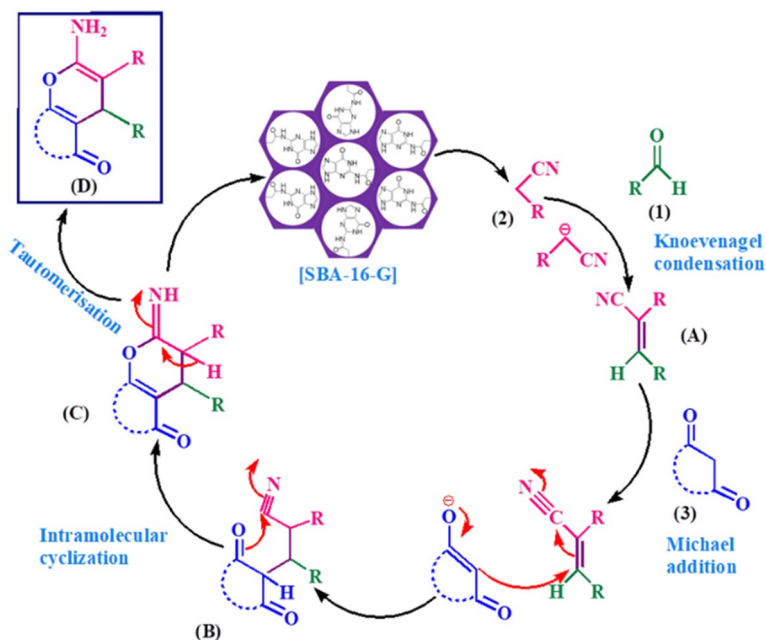


Fig. 6 Plausible mechanism for the synthesis of pyran-annulated heterocyclic compounds

catalytic activities in respect of yields, catalyst loading, reaction times, etc., for the synthesis of pyran-annulated heterocyclic compounds.

Regeneration of [SBA-16-G] catalyst

The catalyst can be regenerated in the dichloromethane solution and dried at 100 °C in a vacuum oven after completion of the reaction. It has been observed that [SBA-16-G] can be reused and is recyclable up to four consecutive cycles without affecting the catalytic efficiency of [SBA-16-G] (SI, Fig. S42). Besides this, FESEM and EDAX analyses (SI, Fig. S43) were carried out to check the changes made in the surface morphology and elemental composition of the spent catalyst. It was observed that the surface morphology and the elemental composition (C, O, Si, and N) of the spent catalyst remained unperturbed.

Plausible mechanism pathway

Based on previous reports [50] and our observations, a plausible mechanism for the synthesis of pyran-annulated via a three-component condensation reaction with [SBA-16-G] is outlined in Fig. 6. The synthetic pathway involves (1) deprotonation of malononitrile/ethylcyanoacetate, (2) Knoevenagel condensation of the aromatic aldehyde with the deprotonated product, (3) Michael addition of intermediate [A] with a C–H activated acidic compound to give product [B], (4) intermediate [B]

undergoing intermolecular cyclization to [C], and (5) tautomerization of intermediate [C] to afford the final pyran-annulated product [D].

Conclusion

In summary, a new solid base, [SBA-16-G], has been synthesized for the first time and fully characterized by FTIR, TGA, XRD, BET, FESEM, EDAX, TEM, CO₂-TPD, and solid-state ¹³C NMR. The [SBA-16-G] showed prominent catalytic activity toward the synthesis of a number of pyran-annulated heterocyclic compounds. The attractive features of this protocol are mild reaction conditions, high yield of products, simple operation, no chromatography, recyclability up to four times, and environmental acceptability of the catalyst due to metal-free catalysis.

Acknowledgements RG and SL acknowledge the Director, IIT (ISM), Dhanbad, for awarding research fellowships. The authors would like to thank CRF at IIT (ISM), Dhanbad, for the FESEM images. We are grateful to Vijay Gupta, SRF, Department of Chemistry, IISER Mohali, Punjab, India, for recording the ¹H and ¹³C NMR data.

References

1. H. Hattori, *J. Jpn. Petrol. Inst.* **47**, 67 (2004)
2. A.S. Matlack, *Introduction to Green Chemistry*, 2nd edn. (CRC Press Taylor & Francis Group, London, 2010), p. 151
3. Y. Ono, T. Baba, *Catal. Today* **38**, 321 (1997)
4. L. Zhu, X.Q. Liu, H.L. Jiang, L.B. Sun, *Chem. Rev.* **117**, 8129 (2017)
5. R. Jothiramalingam, M.K. Wang, *Ind. Eng. Chem. Res.* **48**, 6162 (2009)
6. H. Pines, W.O. Haag, *J. Org. Chem.* **23**, 328 (1958)
7. K. Motahari, A. Salabat, H. Ahmadi, *Fuller. Nanotub. Carbon Nanostruct.* **26**, 342 (2018)
8. Y. Onu, *J. Catal.* **216**, 406 (2003)
9. M. Akizuki, Y. Oshima, *Ind. Eng. Chem. Res.* **57**, 5495 (2018)
10. R. Rinaldi, F. Schuth, *Energy Environ. Sci.* **2**, 610 (2009)
11. E. Safari, A. Hasaninejad, *ChemistrySelect* **3**, 3529 (2018)
12. T. Ebiura, T. Echizen, A. Ishikawa, K. Murai, T. Baba, *Appl. Catal. A* **283**, 111 (2005)
13. A. Marwaha, A. Dhir, S.K. Mahla, S.K. Mohapatra, *Sci. Eng.* **60**, 594 (2018)
14. H. Hattori, *Appl. Catal. A Gen.* **504**, 103 (2015)
15. M. Tang, X. Dou, Z. Tian, M. Yang, Y. Zhang, *Chem. Eng. J.* **355**, 586 (2019)
16. K. Liu, R. Wang, M. Yu, *Renew. Energy* **127**, 531 (2018)
17. V. Chiola, J. E. Ritsko, C.D. Vanderpool, U.S. Patent 3 556 725, 1971
18. S. Sahoo, A. Bordoloi, S.B. Halligudi, *Catal. Surv. Asia* **15**, 200 (2011)
19. F. Tang, L. Li, D. Chen, *Adv. Mater.* **24**, 1504 (2012)
20. H. Sepehrian, J. Fasihi, M.M. Khayatzadeh, *Ind. Eng. Chem. Res.* **48**, 6772 (2009)
21. L. Geng, Y. He, D. Liu, X. Dai, C. Lu, *Microporous Mesoporous Mater.* **148**, 8 (2012)
22. J.A. Melerio, R.V. Grieken, G. Morales, *Chem. Rev.* **106**, 3790 (2006)
23. F. Shieh, C.T. Hsiao, J.W. Wu, Y.C. Sue, Y.L. Bao, Y.H. Liu, L. Wan, M.H. Hsu, J.R. Deka, H.M. Kao, *J. Hazard. Mater.* **206**, 1083 (2013)
24. M. Karin, B. Thomas, *Chem. Mater.* **10**, 2950 (1998)
25. O. Olkhoviyk, M. Jaroniec, *J. Am. Chem. Soc.* **127**, 60 (2005)
26. Y. Zhang, Z.A. Qiao, Y. Li, Y. Liu, Q. Huo, *J. Mater. Chem.* **21**, 17283 (2011)
27. A. Stein, B.J. Melde, R.C. Schroden, *Adv. Mater.* **12**, 1403 (2000)
28. X. Zhuang, Y. Wan, C. Feng, Y. Shen, D. Zhao, *Chem. Mater.* **21**, 706 (2009)

29. S. Zhang, H. Wang, L. Tang, M. Li, J. Tian, Y. Cui, J. Han, X. Zhu, X. Liu, *Appl. Catal. B Environ.* **220**, 303 (2018)
30. S. Zhang, H. Wang, M. Li, J. Han, X. Liu, J. Gong, *Chem. Sci.* **8**, 4489 (2017)
31. M. Waki, Y. Maegawa, K. Hara, Y. Goto, S. Shirai, Y. Yamada, N. Mizoshita, T. Tani, W.J. Chun, S. Muratsugu, M. Tada, A. Fukuoka, S. Inagaki, *J. Am. Chem. Soc.* **136**, 4003 (2014)
32. R. Voss, A. Thomas, M. Antonietti, G. Ozin, *J. Mater. Chem.* **15**, 4010 (2005)
33. M. Lim, C. Blanford, A. Stein, *Chem. Mater.* **10**, 467 (1998)
34. M.E. Davis, *Nature* **417**, 813 (2002)
35. K. Parida, K.G. Mishra, S.K. Dash, *Ind. Eng. Chem. Res.* **51**, 2235 (2012)
36. K. Parida, S.K. Dash, *J. Hazard. Mater.* **179**, 642 (2010)
37. H. Chaudhuri, S. Dash, A. Sarkar, *Ind. Eng. Chem. Res.* **55**, 10084 (2016)
38. P. Das, A. Dutta, A. Bhaumik, C. Mukhopadhyay, *Green Chem.* **16**, 1426 (2014)
39. G. Feuer, in *Progress in Medicinal Chemistry*, ed. by G.P. Ellis, G.P. West (North-Holland Publishing Company, New York, 1974)
40. L. Bonsignore, G. Loy, D. Secci, A. Calignano, *Eur. J. Med. Chem.* **28**, 517 (1993)
41. G.M. Cingolani, F. Gualtteri, M. Pigin, *J. Med. Chem.* **12**, 531 (1961)
42. J.Y.C. Wu, W.F. Fong, J.X. Zhang, C.H. Leung, H.L. Kwong, M.S. Yang, D. Li, H.Y. Cheung, *Eur. J. Pharmacol.* **473**, 9 (2003)
43. P.K. Paliwal, S.R. Jetti, S. Jain, *Med. Chem. Res.* **22**, 2984 (2013)
44. C.W. Smith, J.M. Bailey, M.E.J. Billingham, S. Chandrasekhar, C.P. Dell, A.K. Harvey, C.A. Hicks, A.E. Kingston, G.N. Wishart, *Bioorg. Med. Chem.* **5**, 2783 (1995)
45. Y. Kashman, K.R. Gustafson, R.W. Fuller, J.H. Cardellina, J.B. McMahon, M.J. Currens, R.W. Buckheit, S.H. Hughes, G.M. Gragg, M.R. Boyd, *J. Med. Chem.* **35**, 2728 (1992)
46. P.G. Baraldi, S. Manfredini, D. Simoni, M.A. Tabrizi, J. Balzarini, E.D. Clercq, *J. Med. Chem.* **35**, 1877 (1992)
47. W.O. Foye, *Principi di Chemico Farmaceutica, Piccin* (Padora, Italy, 1991), p. 416
48. L.L. Andreani, E. Lapi, *Bull. Chim. Farm.* **99**, 583 (1960)
49. Y.L. Zhang, B.Z. Chen, K.Q. Zheng, M.L. Xu, X.H. Lei, *Yao Xue Bao* **17**, 17 (1982)
50. L. Bonsignore, G. Loy, D. Secci, A. Calignano, *Eur. J. Med. Chem.* **28**, 517 (1993)
51. G.P. Ellis, in *The Chemistry of Heterocyclic Compounds: Chromenes, Chromanes and Chromones*, ed. by A. Weissberger, E.C. Taylor (Wiley, New York, 1977), p. 11
52. D. Arnesio, W.M. Horspool, N. Martin, A. Ramos, C. Seaone, *J. Org. Chem.* **54**, 3069 (1989)
53. A.T. Khan, M. Lal, S. Ali, MdM Khan, *Tetrahedron Lett.* **52**, 5327 (2011)
54. G. Brahmachari, B. Banerjee, A.C.S. Sustain, *Chem. Eng.* **2**, 411 (2014)
55. J.M. Khurana, B. Nand, P. Saluja, *Tetrahedron* **66**, 5637 (2010)
56. R. Ghorabani-Vaghei, Z. Toghraei-Semiromi, R. Karimi-Nami, *J. Braz. Chem. Soc.* **5**, 905 (2011)
57. S. Balalaie, M. Bararjanian, M. Sheikh-Ahmadi, S. Hekmat, P. Salehi, *Synth. Commun.* **37**, 1097 (2007)
58. Y. Sarrafi, E. Mehrasbi, A. Vahid, M. Tajbakhsh, *Chin. J. Catal.* **33**, 1486 (2012)
59. K. Gong, H.L. Wang, J. Luo, Z.L.J. Liu, *Heterocycl. Chem.* **46**, 1145 (2009)
60. S. Paul, P. Bhattacharyya, A.R. Das, *Tetrahedron Lett.* **52**, 4636 (2011)
61. T.S. Jin, A.Q. Wang, X. Wang, J.S. Zhang, T.S. Li, *Synlett* **5**, 0871 (2004)
62. M. Khoobi, L. Mamani, F. Reza zadeh, Z. Zareie, A. Foroumadi, A. Ramazani, A. Shafiee, *J. Mol. Catal. A Chem.* **359**, 74 (2012)
63. Y. Essamlali, O. Amadine, H. Maati, K. Abdelouahdi, A. Fihri, M. Zahouily, R.S. Varma, A. Solhy, A.C.S. Sustain, *Chem. Eng.* **1**, 1154 (2013)
64. I.A. Azath, P. Puthiaraj, K. Pitchumani, A.C.S. Sustain, *Chem. Eng.* **1**, 174 (2013)
65. A. Montaghami, N. Montazeri, *Orient. J. Chem.* **30**, 1361 (2014)
66. D. Azarifar, M. Tadayoni, M. Ghaemi, *Appl. Organometal. Chem.* **32**, 4293 (2018)
67. A. Dandia, S. Bansal, R. Sharma, V. Parewa, *ChemistrySelect* **3**, 9785 (2018)
68. R.C. Cioc, E. Ruijter, R.V.A. Orru, *Green Chem.* **16**, 2958 (2014)
69. P. Ravichandiran, B. Lai, Y. Gu, *Chem. Rec.* **17**(2), 142 (2016)
70. R. Bai, J. Yang, L. Min, C. Liu, F. Wu, Y. Gu, *Tetrahedron* **72**, 2170 (2016)
71. H. Chaudhuri, R. Gupta, S. Das, *Catal. Lett.* **148**, 1703 (2018)
72. D. Zhao, Q. Huo, J. Feng, B.F. Chmelka, G.D. Stucky, *J. Am. Chem. Soc.* **120**, 6024 (1998)
73. H. Chaudhuri, S. Dash, A. Sarkar, *Ind. Eng. Chem. Res.* **56**, 2943 (2017)
74. A. Alizadeh, M.M. Khodaei, D. Koedsetani, A.H. Fallah, M. Beygzadeh, *Microporous Mesoporous Mater.* **159**, 9 (2012)

75. P.G. Choi, T. Ohno, N. Fukuhara, T. Masui, N. Imanaka, J. Adv. Ceram. **4**, 71 (2015)
76. R. Ouargli-Saker, N. Bouazizi, B. Boukoussa, D. Barrimo, A. Beltrao, A. Azzouz, Appl. Surf. Sci. **411**, 476 (2017)